



# *N*-slit quantum interferometers in the nanometer domain

F. J. Duarte<sup>1</sup> · I. E. Olivares<sup>2</sup>

Received: 13 September 2022 / Accepted: 17 April 2023 / Published online: 9 May 2023  
© The Author(s), under exclusive licence to Springer-Verlag GmbH Germany, part of Springer Nature 2023

## Abstract

*N*-slit quantum interferometers, with dimensions in the micrometer and nanometer range, are designed and theoretically quantified, for the first time to our knowledge, for the detection and characterization of fibers with diameters in the nanometer regime, under x-ray illumination, and in the femtometer regime, under  $\gamma$ -ray illumination.

## 1 Introduction

*N*-slit coherent interferometers, or *N*-slit laser interferometers (NSLI), were first introduced for metrology applications characterizing micro- and nano-structures of imaging and photographic films [1]. Since then, they have been applied to generate interferometric characters for secure space-to-space communications and to the detection of clear air turbulence [2]. Recently, these *N*-slit coherent interferometers have been succinctly mentioned in nanometer dimensions whilst considering  $\gamma$ -ray illumination [2]. In this paper, it is quantitatively shown in detail, via interferometric probability calculations, that such quantum interferometers can be used to determine the diameter of fibers from the nanometer to the femtometer domain. This development points towards the extension of the resolution optical measuring instrumentation, where ‘optical’ is defined as *photon illumination*, beyond current limits.

At present, the resolution of state-of-the-art commercial ‘microscopes’ is in the 10 s of nanometers while commercial electron microscopes go down to a few nanometers. Here, we quantify, via interferometric calculations, resolutions down to the 1 nm regime, using x-ray illumination, and down to the 100 femtometer range under  $\gamma$ -ray illumination. This is the first systematic quantitative assessment of *N*-slit interferometers with nanometer dimensions operating under  $\gamma$ -ray illumination in the open literature.

## 2 Theory

For single-photon illumination, or illumination via an ensemble of indistinguishable photons, the Dirac–Feynman superposition probability amplitude is given by [3–5]

$$\langle d|s \rangle = \sum_{j=1}^N \langle d|j \rangle \langle j|s \rangle, \quad (1)$$

where *s* is the photon source and *d* is the detector or interferometric plane. The index *j* refers to the *j*th slit in the *N*-slit array (*j* = 1, 2, 3...*N*). Under these circumstances either the single photon, or the ensemble of indistinguishable photons, illuminate the *N*-slit array uniformly and simultaneously [1] as depicted in Fig. 1. Detailed experimental descriptions are given in [1, 2].

Following Born’s rule [6], multiplication of (1) with its complex conjugate yields the interferometric superposition probability [1, 2]

$$\langle d|s \rangle \langle d|s \rangle^* = \left( \sum_{j=1}^N \langle d|j \rangle \langle j|s \rangle \right) \left( \sum_{j=1}^N \langle d|j \rangle \langle j|s \rangle \right)^*, \quad (2)$$

which is equivalent to

$$\langle d|s \rangle \langle d|s \rangle^* = \sum_{j=1}^N \Psi(r_j) \sum_{m=1}^N \Psi(r_m) e^{i(\Omega_m - \Omega_j)}, \quad (3)$$

that can also be expressed as

$$|\langle d|s \rangle|^2 = \sum_{j=1}^N \Psi(r_j)^2 + 2 \sum_{j=1}^N \Psi(r_j) \left( \sum_{m=j+1}^N \Psi(r_m) \cos(\Omega_m - \Omega_j) \right). \quad (4)$$

✉ F. J. Duarte  
drfjduarte@gmail.com

<sup>1</sup> Interferometric Optics, Jonesborough, TN, USA

<sup>2</sup> Department of Physics, Universidad de Santiago de Chile, Santiago, Chile

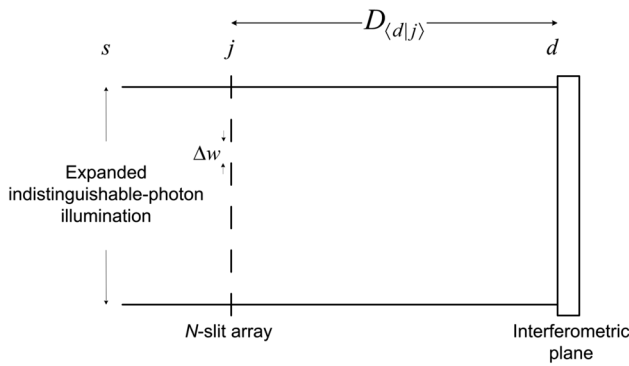


**Fig. 1** Schematics of an  $N$ -slit coherent interferometer: a single-photon, or ensemble of indistinguishable quanta, originates at plane  $s$  and illuminates the whole  $N$ -slit array  $j$ . The interferogram propagates through an intra-interferometric space  $D_{\langle d|j \rangle}$  and is detected, or measured, at the interferometric plane  $d$

Equations (2)–(4) are equivalent quantum probability equations. However, what is measured are intensities. Intensities and quantum probabilities are directly proportional [1, 2, 7]

$$I(v) \propto \langle d|s \rangle \langle d|s \rangle^* \tag{5}$$

In this regard, all the spatial information measured in the intensity profiles is provided via the dimensionless probability. It should be noted that since their very introduction the  $N$ -slit coherent interferometers have been characterized via Dirac’s quantum notation [1].

To our knowledge, this is the first systematic application of the Dirac–Feynman superposition probability amplitude principle in physical dimensions in the sub-nanometer range down to femtometer dimensions while under extremely short wavelength radiation typical of  $\gamma$ -ray illumination.

### 3 Intermediate interferometric plane

There are two alternatives to deal with a new plane inserted in the  $D_{\langle d|j \rangle}$  interferometric path, as illustrated in Fig. 2. The first approach is from the probability amplitude perspective that modifies the original probability amplitude given in (1) so that a new probability amplitude incorporating a new plane, at  $k$ , is introduced [2]

$$\langle d|s \rangle = \sum_{k=1}^N \sum_{j=1}^N \langle d|k \rangle \langle k|j \rangle \langle j|s \rangle, \tag{6}$$

and a new  $\langle d|s \rangle \langle d|s \rangle^*$  probability is calculated.

The second approach involves a cascade method which is a numerical technique introduced in [1] and verified experimentally with excellent results [2]. This cascade

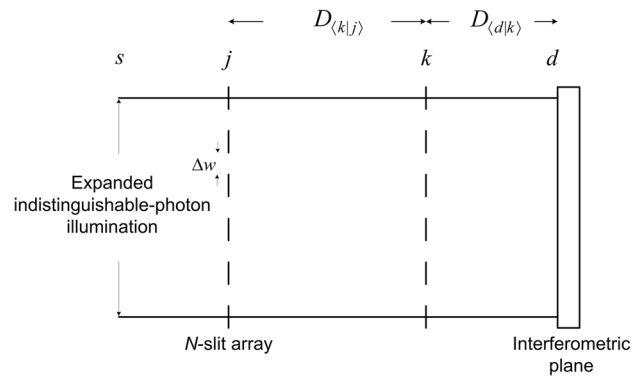


**Fig. 2** Schematics of an  $N$ -slit coherent interferometer incorporating an extra slit array: a single-photon, or ensemble of indistinguishable quanta, originates at plane  $s$  and illuminates the whole  $N$ -slit array  $j$ . The interferogram propagates through an intra-interferometric space  $D_{\langle k|j \rangle}$  and illuminates a second  $N$ -slit array at  $k$ . The new interferogram generated at  $k$  propagates through the intra-interferometric space  $D_{\langle d|k \rangle}$  and is detected, or measured, at the interferometric plane  $d$ . In the present interferometric calculations the  $N$ -slit plane  $k$  is replaced by a single fiber

technique is now explained here for the first time: for the two interferometric planes, depicted in Fig. 2, the illumination probability amplitude at  $k$  is

$$\langle k|s \rangle = \sum_{j=1}^N \langle k|j \rangle \langle j|s \rangle, \tag{7}$$

leading to the probability distribution  $\langle k|s \rangle \langle k|s \rangle^*$ . This new ‘illumination probability’ then becomes the source giving rise to the probability amplitude

$$\langle d|k \rangle = \sum_{j=1}^N \langle d|k' \rangle \langle k'|k \rangle, \tag{8}$$

leading to the final probability on the interferometric plane  $\langle d|k \rangle \langle d|k \rangle^*$ . This is the cascade methodology [1] employed here. The calculated probabilities have the same form as Eqs. (3) and (4). In the present case, the  $N$ -slit array at plane  $k$  is a single cylindrical fiber positioned perpendicular to the illumination plane. This single fiber can be represented as the non-transmission separation of two wide slits.

Confidence for this quantitative analysis is that there is ample data verifying good agreement between calculated interferograms, using (3) and (4), and measured interferograms in the visible spectrum [1, 2]. For instance, the close agreement between theoretical predictions an interferometric measurements in the characterization of a 30  $\mu\text{m}$  transparent spider silk fiber, using  $N$ -slit interferometry, for visible wavelengths is reviewed in detail in [2].

## 4 N-slit quantum interferometer configurations

The first experimental configuration we consider is an x-ray  $N$ -slit interferometer with  $N = 3$ ,  $\lambda = 1$  nm, and  $D_{(dlj)} = 30$   $\mu\text{m}$ . For this interferometer the slits are  $\Delta w = 50$  nm wide, and separated by 50 nm.

The second experimental configuration considered is a  $\gamma$ -ray  $N$ -slit interferometer with  $N = 3$ ,  $\lambda = 100$  fm, and  $D_{(dlj)} = 7.5$  nm. For this interferometer the slits are  $\Delta w = 0.01$  nm wide, and separated by 0.01 nm.

## 5 Available experimental resources

Illumination sources for the x-ray interferometer are presently available from free-electron lasers [8] while  $\gamma$ -ray sources are being investigated via several approaches including plasma irradiation with ultra-intense lasers [9, 10]. An alternative for  $\gamma$ -ray generation is positron–electron annihilation, via  $e^+e^- \rightarrow \gamma_1\gamma_2$ , using deuteron bombardment of  $\text{Cu}^{64}$  [11, 12].

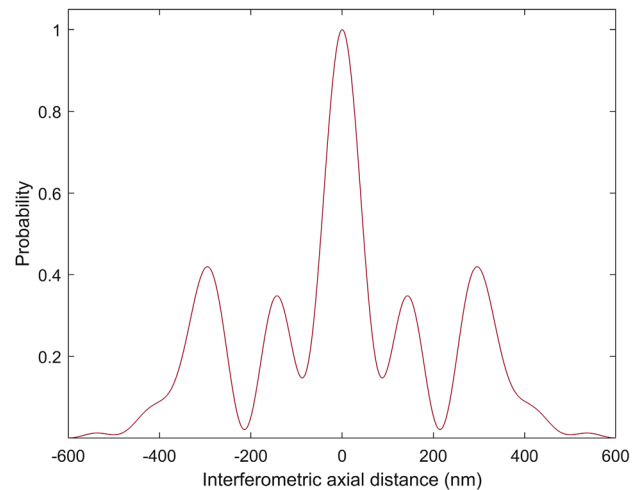
As far as the  $N$ -slit array is concerned: 50 nm slit widths can be achieved via ArF laser lithography [13] and sub-10 nm fabrication appear to be possible [14]. Sub-5 nm dimensions via nanowire arrays have also been reported [15]. However, slit widths in the  $\Delta w = 0.01$  nm range appear beyond present day technology.

## 6 Interferometric results

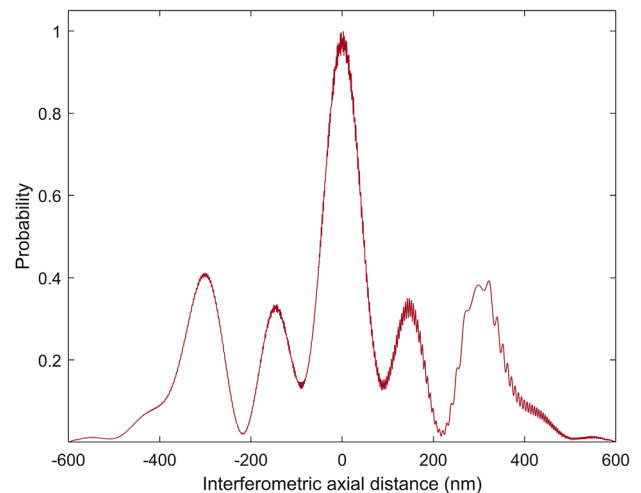
Figure 3 depicts the interferogram calculated for an interferometric configuration consisting of  $N = 3$ ,  $D_{(dlj)} = 30$   $\mu\text{m}$ , under x-ray illumination at  $\lambda = 1$  nm. Figures 4, 5, and 6 are the interferograms calculated while positioning a fiber 0.620  $\mu\text{m}$  from the interferometric plane ( $d$ ) for fiber diameters ( $\varnothing_f$ ) of 1 nm, 5 nm, and 10 nm, respectively.

Figure 7 depicts the interferogram calculated for an interferometric configuration consisting of  $N = 3$ ,  $D_{(dlj)} = 7.5$  nm, under  $\gamma$ -ray illumination at  $\lambda = 100$  fm. Figures 8, 9, and 10 are the interferograms calculated while positioning a fiber 155  $\mu\text{m}$  from the interferometric plane ( $d$ ) for fiber diameters ( $\varnothing_f$ ) of 100 fm, 200 fm, and 300 fm, respectively.

These calculations indicate that these micro- and nano-interferometers can clearly differentiate set of fibers in the  $1 \leq \varnothing_f \leq 10$  nm range, for the 30  $\mu\text{m}$  configuration, and in the  $100 \leq \varnothing_f \leq 300$  fm range, for the 7.5 nm configuration.



**Fig. 3**  $N$ -slit coherent interferogram for  $N = 3$ ,  $\Delta w = 50$  nm,  $\lambda = 1$  nm, and  $D_{(dlj)} = 30$   $\mu\text{m}$ . This becomes the ‘control interferogram’ for this configuration



**Fig. 4**  $N$ -slit coherent interferogram for  $N = 3$ ,  $\Delta w = 50$  nm,  $\lambda = 1$  nm, and  $D_{(dlj)} = 30$   $\mu\text{m}$ . In this case, a fiber with a diameter of  $\varnothing_f = 1$  nm is introduced, perpendicular to the plane of propagation, at an intra-interferometric distance of 620 nm from the interferometric plane  $d$ . The lateral position of the fiber is 290 nm to the right of 0 on the interferometric plane

## 7 Discussion

Observing the interferograms displayed in Figs. 4, 5 and 6, it is evident that the 30  $\mu\text{m}$  interferometer clearly differentiates between the 1 nm, 5 nm, and 10 nm fibers. For  $\lambda = 1$  nm, and for the present interferometric configuration, the resolution of the 30  $\mu\text{m}$  interferometer appears to be in the 1 nm range.

Evaluation of the interferograms displayed in Figs. 8, 9 and 10 indicates that the 7.5 nm interferometer clearly

**Fig. 5**  $N$ -slit coherent interferogram for  $N = 3$ ,  $\Delta w = 50$  nm,  $\lambda = 1$  nm, and  $D_{(d_{ij})} = 30$   $\mu\text{m}$ . In this case, a fiber with  $\varnothing_f = 5$  nm is introduced, perpendicular to the plane of propagation, at an intra-interferometric distance of 620 nm from the interferometric plane  $d$ . The lateral position of the fiber is 290 nm to the right of 0 on the interferometric plane

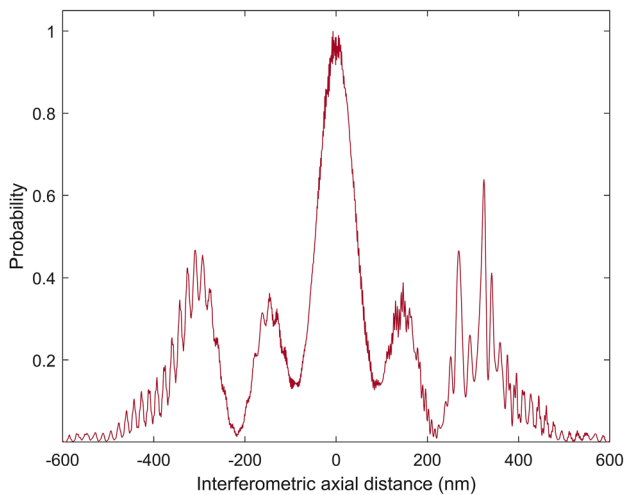
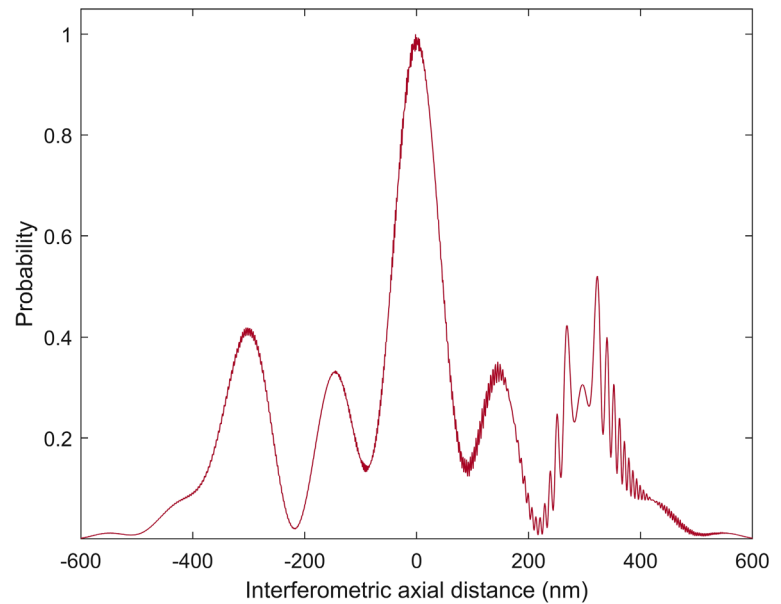


**Fig. 6**  $N$ -slit coherent interferogram for  $N = 3$ ,  $\Delta w = 50$  nm,  $\lambda = 1$  nm, and  $D_{(d_{ij})} = 30$   $\mu\text{m}$ . In this case, a fiber with  $\varnothing_f = 10$  nm is introduced, perpendicular to the plane of propagation, at an intra-interferometric distance of 620 nm from the interferometric plane  $d$ . The lateral position of the fiber is 290 nm to the right of 0 on the interferometric plane

differentiates between the 100 fm, 200 fm, and 300 fm fibers. For  $\lambda = 100$  fm, and for the present interferometric configuration considered here, the resolution of the 7.5 nm interferometer appears to be in the 100 fm range.

As expected, the resolution of these micro- and nano-interferometers is limited by the wavelength of the illumination.

Albeit construction of the 7.5 nm interferometer appears to be beyond present technological capabilities, construction of a 30  $\mu\text{m}$  interferometer appears feasible utilizing available

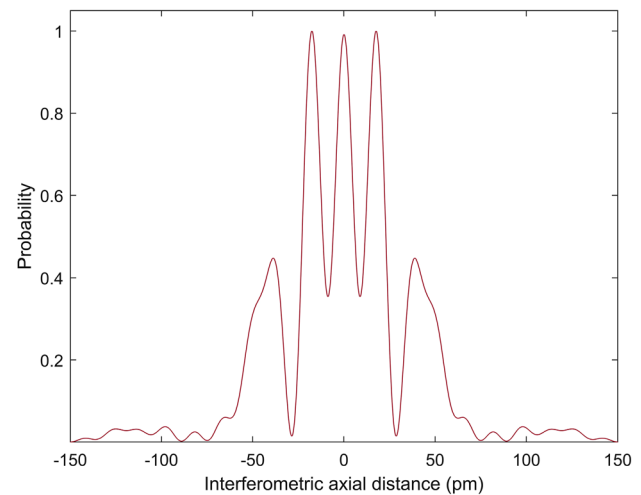


**Fig. 7**  $N$ -slit coherent interferogram for  $N = 3$ ,  $\Delta w = 0.01$  nm,  $\lambda = 100$  fm, and  $D_{(d_{ij})} = 7.5$  nm. This becomes the ‘control interferogram’ for this configuration

free-electron laser technology and laser lithography technology. Besides, what has been demonstrated here is that the measurement range and scope of quantum optical measurement instrumentation can be down-extended beyond present limits utilizing compatible interferometric dimensions with given, or available, wavelengths.

The calculations presented in this paper represent the first characterization of nanometer-range  $N$ -slit interferometers capable of differentiating spatial features down in the femtometer range. This initial step should open new avenues for the engineering and fabrication of such interferometers. Furthermore, this introduces the concept of a new metrology tool based on sound physical principles in nanoengineering

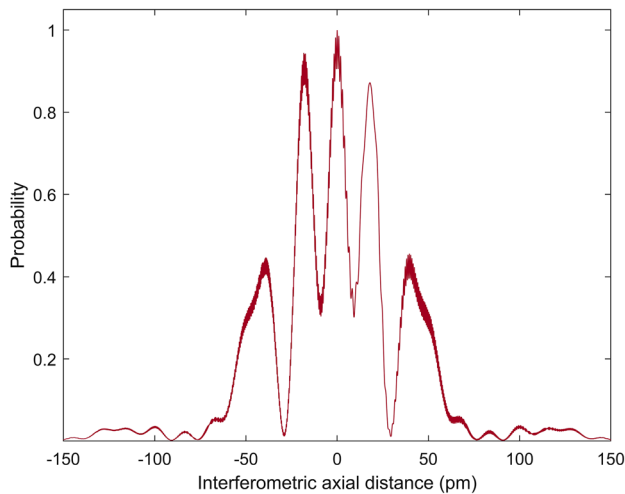


**Fig. 8**  $N$ -slit coherent interferogram for  $N = 3, \Delta w = 0.01$  nm,  $\lambda = 100$  fm, and  $D_{(dlj)} = 7.5$  nm. In this case, a fiber with  $\varnothing_f = 100$  fm is introduced, perpendicular to the plane of propagation, at an intra-interferometric distance of 155 pm from the interferometric plane  $d$ . The lateral position of the fiber is 17.4 pm to the right of 0 on the interferometric plane

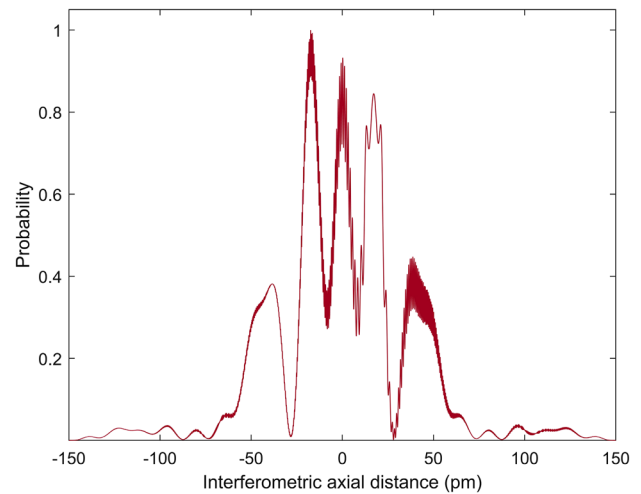


**Fig. 10**  $N$ -slit coherent interferogram for  $N = 3, \Delta w = 0.01$  nm,  $\lambda = 100$  fm, and  $D_{(dlj)} = 7.5$  nm. In this case, a fiber with  $\varnothing_f = 300$  fm is introduced, perpendicular to the plane of propagation, at an intra-interferometric distance of 155 pm from the interferometric plane  $d$ . The lateral position of the fiber is 17.4 pm to the right of 0 on the interferometric plane

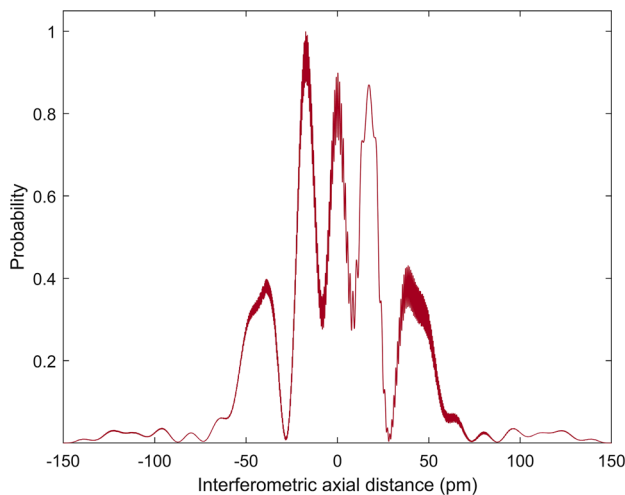


**Fig. 9**  $N$ -slit coherent interferogram for  $N = 3, \Delta w = 0.01$  nm,  $\lambda = 100$  fm, and  $D_{(dlj)} = 7.5$  nm. In this case, a fiber with  $\varnothing_f = 200$  fm is introduced, perpendicular to the plane of propagation, at an intra-interferometric distance of 155 pm from the interferometric plane  $d$ . The lateral position of the fiber is 17.4 pm to the right of 0 on the interferometric plane

where, for instance, the characterization of nanowires [16] and nanofibers [17] is desired. As Richard Feynman said: “there is plenty of room at the bottom” [18].

**Acknowledgements** The authors would like to thank a reviewer for critical comments leading to the conceptual clarification of the original manuscript. One of us (IEO) acknowledges the support of DICYT Project Code 042031OB.

**Author contributions** FJD is the author of the  $N$ -slit interferometric theory and designer of the interferometers. IOE performed the numerical calculations. Both authors contributed equally to the manuscript.

**Funding** This work was partially funded, in regard to IOE, by DICYT Project Code 042031OB.

**Data Availability** The precise quote by R P Feynman (from the cited reference) is: “There is plenty of room at the bottom”.

## Declarations

**Conflict of interest** The authors declare no conflict of interest.

## References

1. F.J. Duarte, Opt. Commun. **133**, 8 (1993)
2. F. J. Duarte, *Fundamentals of Quantum Entanglement*, 2nd edn (Institute of Physics, Bristol, 2022)
3. P.A.M. Dirac, Math. Proc. Cam. Philos. Soc. **35**, 416 (1939)
4. P.A.M. Dirac, *The Principles of Quantum Mechanics*, 4th edn. (Oxford University, Oxford, 1958)
5. R. P. Feynman, R. B. Leighton, M. Sands, *The Feynman Lectures on Physics*, Vol. III (Addison-Wesley, Reading, 1965)
6. M. Born, Z. Phys. **37**, 863 (1926)
7. M. Sargent, M. O. Scully, and W. E. Lamb, *Laser Physics* (Addison-Wesley, Reading, 1974).
8. J. B. Rosenzweig, N. Majernik, R. R. Robles, G. Andonian, O. Camacho, A. Fukawa, A. Kogar, G. Lawler, J. Miao, P. Musumeci, B. Naranjo, Y. Sakai, R. Candler, B. Pund, C. Pellegrini, C. Emma, A. Halavanau, J. Hastings, Z. Li, M. Nasr, S. Tantawi, P. Anisimov, B. Carlsten, F. Frawczyk, L. Faillace, M. Ferrario, B. Spataro, S. Karkare, J. Maxson, Y. Ma, J. Wurlete, A. Murokh, A. Zholents, A. Cianchi, D. Cocco, and S. B. van der Geer, New J. Phys. **22**, 093067 (2022)

9. X.-B. Wang, G.-Y. Hu, Z.-M. Zhang, Y.-Q. Gu, B. Zhao, Y. Zuo, and J. Zheng, *High Power Laser Sci. Eng.* **8**, e34 (2020)
10. A. Sampath et al., *Phys. Rev. Lett.* **126**, 064801 (2021)
11. R.C. Hanna, *Nature* **162**, 332 (1948)
12. C. S. Wu and I. Shakhov, *Phys. Rev.* **77**, 136 (1950)
13. J. Song, J.S. Oh, M.J. Bak, I.-S. Kang, S.J. Lee, G.-W. Lee, *Nanomaterials* **12**, 481 (2022)
14. Y. Shen, Z. Shu, S. Zhang, P. Zeng, H. Liang, M. Zheng, H. Duan, *Int. J. Extreme Manuf.* **3**, 032002 (2021)
15. S. Gao, S. Hong, S. Park, H.Y. Jung, W. Liang, Y. Lee, C. W. Ahn, J. Y. Byun, J. Seo, M. G. Hahm, H. Kim, K. Kim, Y. Yi, H. Wang, M. Upmanyu, S-G. Lee, Y. Homma, H. Terrones, and Y. J. Jung, *Nat. Commun.* **13**, 3467 (2022)
16. C.A. Ritcher, H.D. Xiong, X. Zhu, W. Wang, V.M. Stanford, W.-K. Hong, T. Lee, D.E. Ioannou, Q. Li, *IEEE Trans. Electron. Dev.* **55**, 3086 (2008)
17. L. Hiremath, K.S. Narendra, K.G. Praveen, K.S. Ajeet, C. Shreya, R. Suresh, E. Keshamma, *J. Pure Appl. Microbiol.* **13**, 2129 (2019)
18. R.P. Feynman, *Eng. Sci.* **23**(5), 22 (1960)

**Publisher's Note** Springer Nature remains neutral with regard to jurisdictional claims in published maps and institutional affiliations.

Springer Nature or its licensor (e.g. a society or other partner) holds exclusive rights to this article under a publishing agreement with the author(s) or other rightsholder(s); author self-archiving of the accepted manuscript version of this article is solely governed by the terms of such publishing agreement and applicable law.